

## 1 **Flow-Substrate Interactions in Aggrading and Degrading Submarine Channels**

2 **Anjali M. Fernandes<sup>1,2</sup>, James Buttles<sup>1</sup>, David Mohrig<sup>1</sup>**

3 *<sup>1</sup>The Center for Integrative Geoscience, University of Connecticut, Storrs, Connecticut, USA.*

4 *<sup>2</sup>The Jackson School of Geosciences, The University of Texas at Austin, Texas, USA.*

5 *Email: [anjali.fernandes@uconn.edu](mailto:anjali.fernandes@uconn.edu)*

6 **Keywords:** Turbidity currents; submarine channels; submarine canyons; boundary layer roughness; flow-  
7 separation zones; erosional bedforms; detachment-limited channels; transport-limited channels; Shields  
8 scaling

### 9 **ABSTRACT**

10 Connecting real time measurements of current-bed interactions to the temporal evolution of  
11 submarine channels can be extremely challenging in natural settings. We present a suite of physical  
12 experiments that offer insight into the spectrum of interactions between turbidity currents and their  
13 channels, from (i) detachment-limited erosion to (ii) transport-limited erosion to (iii) pure deposition. In  
14 all three cases channel sinuosity influenced patterns of erosion and deposition; the outsides of bends  
15 displayed the highest erosion rates in the first two cases, whereas the outsides of bends were associated  
16 with the highest deposition rates the third. We connect the evolution of these channels to the turbulence of  
17 the near-bed boundary layer. In the erosional experiments both channel beds roughened through time,  
18 developing erosional bedforms or trains of ripples. Reynolds estimates of boundary layer roughness  
19 indicate that, in both erosional cases, the near-bed boundary layer roughened from smooth or  
20 transitionally rough to rough, whereas the depositional channel appears to have remained consistently  
21 smooth. Our results suggest that, in the absence of any changes from upstream, erosion in submarine  
22 channels is a self-reinforcing mechanism whereby developing bed roughness increases turbulence at the  
23 boundary layer, thereby inhibiting deposition, promoting sediment entrainment and enhancing channel

24 relief; deposition occurs in submarine channels when the boundary layer remains smooth, promoting  
25 aggradation and loss of channel relief.

## 26 **INTRODUCTION**

27 Continental margins are patterned with channels and canyons that convey large volumes of  
28 sediment to the deep ocean. These channels evolve through erosion and/or deposition, often aggrading  
29 over significant vertical distances (Pirmez et al., 2000), or by carving canyons (Babonneau et al., 2010;  
30 Conway et al., 2012) many hundreds of meters deep. Physical experiments can offer insight into current-  
31 bed interactions. Such measurements are challenging to acquire in natural settings and even more  
32 challenging to relate to the temporal evolution of submarine channels (Khripounoff et al., 2003; Xu et al.,  
33 2004, 2013; Xu, 2010; Hughes Clarke, 2016; Symons et al., 2017; Azpiroz-Zabala et al., 2017b, 2017a).  
34 In the past, some experiments e.g. (Mohrig and Buttle, 2007; Straub et al., 2008; Janocko et al., 2013)  
35 focused on purely depositional turbidity currents that were suspension-dominated, whereas others  
36 investigated erosional currents that modified channels primarily through bedload-transport (Métivier et  
37 al., 2005; Amos et al., 2010). Here we present three experiments which we use to explore the processes  
38 that shape submarine channels, along the continuum of intensely erosional to purely depositional in  
39 connection to the hydraulic characteristics of the near-bed boundary layer, across this spectrum of  
40 behavior.

### 41 **Detachment-limited and transport-limited erosion in terrestrial landscapes**

42 Terrestrial channels eroding into bedrock have been modeled using: a) a detachment-limited model  
43 in which the resistance of the substrate is the limiting factor that controls the erosion rate, and b) a transport-  
44 limited model where the erosion rate is limited by the ability to transport the eroded sediment (Howard,  
45 1980, 1994; Whipple, 2004). Detachment-limited erosion is more sensitive to local conditions (e.g.  
46 topographic or bed roughness) rather than reach-averaged conditions (e.g. discharge; (Johnson and  
47 Whipple, 2007)). Erosion generally takes place through abrasion and wear by the impacts of sediment being  
48 transported by the flow, and turbulence generated by evolving bed roughness. These channels are

49 characterized by knickpoints, inner channels, scour holes, grooves, and sculpted bedforms (Whipple, 2004).  
50 The transporting currents are efficient at removing sediment in transport from upstream and at entraining  
51 material from the local substrate.

52         When the removal of eroded sediment is not efficient, sediment is stored in patches on the bed,  
53 protecting the bed from further erosion in a phenomenon referred to as the ‘cover-effect’ (Johnson et al.,  
54 2009). Erosional channels with abundant sediment cover on the channel bed are referred to as “transport-  
55 limited” (Shepherd and Schumm, 1974; Sklar and Dietrich, 2004; Whipple, 2004; Johnson and Whipple,  
56 2007). Partially-alluviated erosional channels scouring into compact, indurated sediment have been  
57 observed in depositional landscapes such as the Mississippi River Delta (Edmonds et al., 2011; Nittrouer  
58 et al., 2011a), where cover effects are particularly evident. Channel bottoms display deep scours where they  
59 are devoid of alluvial cover at the outsides of river bends. All natural erosional channels can be expected to  
60 display some combination of detachment-limited and transport-limited behavior (Whipple, 2004). Here we  
61 use 2 experiments to study the characteristics of detachment-limited and transport-limited erosion in  
62 submarine channels. For completeness, we incorporate data from an aggradational channel experiment  
63 (Straub et al., 2008). We use these experiments to explore the role of the near-bed boundary layer in the  
64 spectrum of forms and deposit characteristics observed.

### 65 **Dynamic scaling of experiments to natural systems**

66         Laboratory experiments have historically been compared to natural systems by using three  
67 dimensionless variables: (1) the densimetric Froude number ( $Fr_d$ ), (2) the Reynolds number ( $Re$ ), and (3)  
68 the ratio of current shear velocity  $u^*$  to particle fall velocity  $w_s$  (Middleton, 1966; Baas et al., 2004; Yu et  
69 al., 2006; Mohrig and Buttle, 2007; Straub et al., 2008; Amos et al., 2010; Rowland et al., 2010; Cantelli  
70 et al., 2011). The first parameter, the Froude number, defines the ratio between momentum and  
71 gravitational forces within the transporting current and is traditionally maintained equal or similar to  
72 natural analogues. The Reynolds number, which quantifies the turbulence of the currents, cannot be equal  
73 to natural flows in scaled-down laboratory settings. The third parameter, also referred to as a Shield’s

74 parameter (Shields, 1936; Bagnold, 1966; Smith and Hopkins, 1971; van Rijn Leo C., 1984; Nino et al.,  
75 2003), characterizes how sediment is transported. Flows in which the turbulent shear, expressed as the  
76 shear velocity  $u^*$ , is significantly larger than the gravitational settling velocity  $w_s$  will be more competent  
77 at transporting sediment in suspension over significant distances (Shields, 1936; Smith and Hopkins,  
78 1971) and will preclude sediment-bed interactions over short length scales; if  $u^*$  is comparable to  $w_s$ ,  
79 sediment can be transported as either saltating or incipiently suspended load, dependent upon the intensity  
80 of turbulence associated with current-bed interactions. In channelized turbidity currents, the intensity of  
81 near-bed turbulence is the combined result of turbulent eddies shed at the scale of individual particles (de  
82 Leeuw et al., 2016), of bed roughness (e.g. bedforms, scours, etc.) (Eggenhuisen et al., 2010;  
83 Eggenhuisen and McCaffrey, 2012; Arfaie et al., 2018), as well as of planform irregularities (e.g. curved  
84 channels) (Straub et al., 2011) which can impart turbulent shear from non-uniform spatial accelerations.  
85 The magnitude of turbulence will scale with the magnitudes of fluid shear ( $u^*$ ) and the size of the element  
86 under consideration (e.g. particle diameter, dune height, scour depth, bend amplitude, etc.). Turbulence  
87 associated with these roughness scales contributes to entrainment of sediment from the bed and walls of  
88 channels, and encourages vertical mixing which maintains sediment in suspension. The ratio between  
89 fluid shear and the viscous forces which act to damp turbulence can be used to characterize the roughness  
90 of the near-bed boundary layer (Garcia, 2008).

91 De Leeuw et al. (2016) argued that realistic turbulence-sediment interactions were critical for  
92 effectively modelling submarine channel inception and evolution, and proposed a scaling approach defined  
93 by the ratio of the Shield's parameter to the particle Reynolds number ( $Re_p$ ). In this scaling approach, the  
94 Shield's parameter is held similar between experimental and naturally occurring density currents, but the  
95 similarity between the particle Reynolds numbers is relaxed as long as the boundary layer is rough or  
96 transitionally rough (Garcia, 2008; de Leeuw et al., 2016). Leeuw et al. (2017) noted that density currents  
97 in most previous experiments were highly depositional because the boundary layers were hydraulically  
98 smooth and/or the Shields parameter fell below the initiation of suspension.

99            In Figure 1, we adopt the Shield's scaling proposed by de Leeuw et al. (2016) to compare flow and  
100 sediment transport characteristics of the three experiments presented here to past experimental and field  
101 measurements. Although the shear stresses associated with all three experiments exceeded the threshold for  
102 the initiation of suspension, they straddle the threshold between hydraulically smooth and transitionally  
103 rough boundary layers. Furthermore, Experiments 1 and 2 scale best with recent field observations of flow  
104 and transport in natural systems. Using sediment with much lower densities than silica in these experiments  
105 allowed us to use sand-sized particles that had transitionally rough boundary layers and high Shields  
106 parameters, and were therefore easy to suspend and maintain in suspension.

### 107 **Experiment Design**

108            In each experiment, calcium chloride salt and water (and sediment, when it was used), were mixed  
109 together in a reservoir, until the salt was completely dissolved. The mixture was agitated over several hours  
110 and allowed to cool to room temperature, as the dissolution of this salt in water is an exothermic process.  
111 Once at room temperature, the mixture was pumped up to a constant head tank and then allowed to flow  
112 into the experimental basin at a controlled rate set by the constant hydraulic head and a system of valves.  
113 The two experimental basins were designed along similar lines, shown by the generalized schematic in  
114 Figure 2. In all experiments, density currents were released into an experimental channel through a box  
115 with two perforated screens designed to extract momentum from flows. The pre-formed channels were built  
116 upon a platform separated from the walls of the basin by deep moats that prevented currents from reflecting  
117 off the basin walls. Saline fluid was not allowed to collect in the basin and was extracted through the floor  
118 drains as it flowed off the raised platform. The water level in the basin was maintained with a constant flux  
119 of fresh water and overflow drainage through a weir. The basin used in Experiment 1 was 8 m long, 6 m  
120 wide and 2 m deep. The basin used for Experiments 2 & 3 was 5 m long, 4.5 m wide and 0.8 m deep. In all  
121 experiments, the channel was constructed diagonally across the false floor.

122            The channels used in these experiments were designed with similar sinuosity, but different  
123 sediment and flow properties (Table 1). In Experiment 1, the channel was built entirely out of a weakly  
124 cohesive mixture of acrylic particles (specific gravity = 1.15) and clay positioned on top of a sloping ramp.

125 The sediment was mixed in a 10:1 volumetric ratio. The first two currents released into the channel were  
 126 saline density currents (excess density = 4%). These were followed by three more density currents that  
 127 carried a 2% volumetric concentration of suspended acrylic sediment.

128 In Experiment 2 a saline density current (excess density = 3.32%) was released through the  
 129 experimental channel which consisted of a cohesionless, 2-cm thick bed of acrylic particles draped over a  
 130 sinuous channel form built from concrete. In Experiment 3 sixteen purely depositional currents flowed  
 131 through a channel constructed of concrete with a thin layer of silica sediment on the bed. Currents had an  
 132 excess density of 2.1%. 33% of this excess density was supplied by suspended sediment in the current, and  
 133 the remaining 67% was from dissolved salt. High-resolution bathymetry maps (horizontal resolution =  
 134 4mm; vertical resolution ~100 microns for Experiments 1 & 2; ~1mm for Experiment 3), collected before  
 135 and after each flow defined patterns of bed change for all three cases. Key geometric and dynamic properties  
 136 of the experimental designs are compiled in Table 1.

137 **Table 1: Summary of geometric and dynamic properties of Experiments 1, 2 and 3.**

	Parameter	Experiment 1	Experiment 2	Experiment 3
Channel geometry	Channel depth (m)	0.15	0.09	0.11
	Channel width (m)	0.50	0.40	0.40
	Down-channel slopes (degrees)	7.00	2.00	1.00
	Initial mean thickness of erodible bed (m)	0.07	0.02	0.00
	Channel sinuosity	1.15	1.28	1.28
Sediment properties	Sediment density ( $\rho_s$ ) (kg/m <sup>3</sup> )	1150.00	1150.00	2650.00
	D <sub>1</sub>	49	49	1.7
	D <sub>10</sub>	88	88	12.9
	D <sub>25</sub>	127	127	23
	D <sub>50</sub>	146	146	31
	D <sub>75</sub>	205	205	41
	D <sub>90</sub>	243	243	52.1
	D <sub>99</sub>	340	340	80
Flow properties	Flow thickness (m)	0.10	0.09	0.10
	Current density ( $\rho_f$ ) (kg/m <sup>3</sup> )	1040	1033.20	1021
	Depth-averaged downstream velocity (u) (m/s)	0.10	0.05	0.08
	Shear velocity (u*) (m/s)	0.04	0.03	0.04
	Froude number (Fr)	0.50	0.26	0.56
	Reynolds number (Re)	10000.00	4050.00	8000.00
	Particle Reynolds number (Re <sub>p</sub> )	6.53	4.38	1.24
	Shields parameter	13.20	5.56	3.30
	Bed roughness scale (H <sub>bed</sub> ) (m)	0.01 - 0.05	0.01 - 0.02	-
Reynolds number from bed roughness (Re <sub>bed</sub> )	~650 - 2236	~330- 660	-	

138

## 139 **Results**

140 Integrating surface change for each flow in all three cases reveal net erosion in Experiments 1 and  
141 2, and net deposition in Experiment 3.

### 142 **Experiment 1**

143 In Experiment 1, all 5 currents released through the channel modified it through net erosion (Fig.  
144 3 A, Fig. 4). The weakly cohesive bed consisted of sediment that was easily suspended once it detached  
145 from the surface (Fig. 1). Extreme run-up of currents onto the outer walls of channel bends occurred,  
146 resulting in the formation of a low-velocity flow-separation zone (depth-averaged velocity  $\sim$  1-2 m/s) at  
147 the inner bank (Fig. 4G; Fig.5) (Leeder and Bridges, 1975; Fernandes et al., 2018). Erosion occurred  
148 beneath the pathway of the high-velocity (depth-averaged velocity = 10m/s) core of the current, which  
149 travelled along the outside of bends and created a series of discontinuous scours. Initially, while the channel  
150 bed was smooth, the most intense scouring occurred at the outside of bends (Fig. 4A, B, H; Fig. 6).  
151 Subsequently, the rough edges of scours became sites of focused erosion (Fig. 4C-F, I-L; Fig. 6A-C) and  
152 resultant elongation of scours resulted in the formation of a discontinuous inner channel (Fig. 7A- B).  
153 Focused erosion at the downstream edges of scours released clouds of suspended sediment that were  
154 transported downstream and out of the system. Consecutive inner bank areas were separated by a swath of  
155 erosion, and evolved into raised terraces within the low-velocity flow separation zone (Fig. 3A, Fig. 4;  
156 (Fernandes et al., 2018). The channel bed evolved from smooth to ornamented, displaying erosional  
157 bedforms with centimeter-scale relief (Fig. 3A; Fig. 6). These bed morphologies are similar to those  
158 observed in detachment-limited terrestrial channels, where erosion is limited by the strength of the substrate  
159 and bed erosion occurs primarily through wear by abrasion and plucking (Whipple et al., 2000; Whipple,  
160 2004). The channel remained net-erosional through its entire length (Fig. 3A; Fig. 4).

### 161 **Experiment 2**

162           This channel was modified through net-erosion, with a fraction of mobilized sediment leaving the  
163 system in suspension while the remainder was reworked into a continuous train of bedforms (Fig. 3B). As  
164 in Experiment 1, the high velocity core of the density current travelled along the outsides of bends, resulting  
165 in: 1) erosion of sediment at the outer bank, where sediment removal exposed the underlying erosion-  
166 resistant channel form in the troughs between sediment-starved bedforms, and 2) deposition at the inner  
167 bank, which resulted from the convergence of downstream and cross-stream bedload transport (Fig. 3B,  
168 Fig 7C-D). These zones of deposition began just upstream from the points of maximum channel curvature,  
169 and were connected across inflection points through the continuous bedform field (Fig. 4B). Erosion in this  
170 experiment was less efficient than in Experiment 1. Abundant sediment cover on the channel bed is  
171 suggestive of erosional mechanics similar to that of transport-limited erosional terrestrial channels, which  
172 are also characterized by alluviated channel beds interrupted by variable degrees of local scouring  
173 (Whipple, 2004; Nittrouer et al., 2011a, 2011b), and in which the erosion rate is limited by the ability of  
174 the flow to transport the eroded sediment.

### 175 **Experiment 3**

176           Currents modified this channel via net sediment deposition (Straub et al., 2008). The thickest  
177 deposition closely tracked the pathway of the high velocity core, which was inferred to be the pathway of  
178 the highest suspended sediment concentration (Fig. 9 of Straub et al., 2008). This resulted in thicker deposits  
179 at the outer banks of bends and thinner deposits in low-velocity zones at the inner banks of bends (Fig. 3C,  
180 Fig. 7E-F). Deposits from each current draped the entire channel (Fig. 7E-F), and thinned in the downstream  
181 direction (Fig. 6D-F). Sediment was primarily transported as and deposited from suspended load.  
182 Suspended sediment flux was estimated to be roughly 40 times that of bedload flux (Straub et al., 2008).

### 183 **Discussion**

#### 184 **Boundary layer roughness in erosional and depositional channels**



185           The transporting currents in all three experiments had shear stresses that were high enough to  
186 transport sediment in suspension. Yet their temporal evolution spanned the spectrum from intense erosion  
187 to pure deposition. In all three cases, planform irregularity influenced the spatial variability in sedimentation  
188 and/or erosion by influencing the path of the highest velocities and sediment concentrations. A key  
189 difference between the 3 experiments lies in the characteristics of the hydraulic boundary layer and the  
190 temporal evolution of the three channels suggests strong agreement with the Shield-scaling predictions of  
191 de Leeuw et al., 2016. Particle-scale Reynolds estimates of boundary layer turbulence place Experiment 1  
192 in the transitionally rough hydraulic regime, whereas Experiment 2 was at the approximate boundary  
193 between the smooth and transitionally rough regime, and Experiment 3 was squarely within the  
194 hydraulically smooth regime. Furthermore, Experiment 1 evolved from a smooth bed to one patterned by  
195 scours, grooves and other centimeter-scale erosional bedforms; Experiment 2 evolved from a smooth bed  
196 into a semi continuous bedform field. In both erosional experiments the roughening of the channel bed is  
197 likely to have encouraged greater turbulence at the near-bed boundary (Fig. 2).

198           At the start of Experiment 1, the smooth sediment bed was modified by erosion along the pathway  
199 of the high velocity core; the magnitude of erosion appeared to be greatest near the outsides of bends (Fig.  
200 4A, B, G, H). Particle Reynolds numbers calculated from mean, depth-averaged downstream velocities at  
201 the outsides (0.1 m/s) and insides (0.01 - 0.02 m/s) of bends point to a hydraulically smooth boundary layer  
202 within the flow separation zone at the inside of the bend, and a transitionally rough boundary layer at the  
203 outside (Fig. 2). The emergence of erosional roughness with 1-5 centimeter relief is likely to have further  
204 roughened the boundary layer, prohibiting sediment deposition and increasing erosion at sites with  
205 enhanced roughness (Fig. 3A; Fig. 4; Fig.6). Near bed turbulence increased by at least two orders of  
206 magnitude ( $Re_{bed} \sim 450$  for 1cm relief;  $Re_{bed} \sim 2200$  for 5cm relief; Fig. 2), causing a regime shift towards  
207 a hydraulically rough boundary layer (Garcia, 2008). Hydraulically smooth boundary layers in flow  
208 separation zones at the inner banks (Fig. 2) precluded erosion and very low suspended sediment fluxes were  
209 unfavorable for deposition. Overall, Experiment 1 evolved in such a way that sediment entrainment and

210 removal remained efficient through time, and channel relief consistently increased as currents scoured into  
211 the ~7cm thick erodible sediment bed (Fig. 6A; Fig 7A). Detachment-limited erosion is indicated by  
212 evolution of sculpted erosional bedforms, efficient sediment removal and enhanced erosion linked to local  
213 bed roughness. The temporal evolution of this channel therefore offers significant insights into the evolution  
214 of topography and flow-bed interactions in detachment-limited erosional submarine channels and canyons  
215 e.g. (Conway et al., 2012; Vachtman et al., 2013; Mitchell, 2014) that incise into compacted or indurated  
216 fine-grained sediment on the upper continental slope and are efficient, dominantly-erosional conduits for  
217 sediment transport into the deep ocean.

218         Like Experiment 1, Experiment 2 also evolved from a smooth bed to a rough one and the outer  
219 banks of bends were sites of enhanced erosion. Using ripple crest height of 1-2 cm as the relevant length  
220 scale, Reynolds estimates indicate that the boundary layer evolved to become hydraulically rough (Fig. 2;  
221 (Garcia, 2008), though it was at the threshold between hydraulically smooth and transitionally rough at the  
222 start of the experiment (Table 1). The Shields parameter for all particle sizes present falls above the  
223 threshold for initiation of suspension (Shields, 1936; Bagnold, 1966; Smith and Hopkins, 1971; van Rijn  
224 Leo C., 1984; Nino et al., 2003), suggesting that the rate of erosion was limited by the currents' capacity to  
225 transport the sediment in suspension, and that the sediment that could not be suspended was transported as  
226 bedload. The development of a bedform field, while it likely facilitated sediment entrainment by roughening  
227 the boundary layer probably also reduced fluid momentum and the capacity of the current to suspend  
228 sediment. This style of transport-limited erosion (Whipple, 2004; Johnson and Whipple, 2007) likely offers  
229 insight into the delicate balance of flow-sediment feed-backs that control spatially variable sedimentation  
230 and erosion in dominantly bypassing submarine channels on the middle or lower continental slope.

231         Unlike Experiments 1 and 2, Experiment 3 remained depositional for the duration of the  
232 experiment. Straub et al., (2008) noted that super-critically climbing ripples were present over only  
233 approximately 5% of the sediment bed. Consistent deposition and reduction in channel relief (Straub et al.,  
234 2008) through time suggests that the boundary layer characteristics likely shifted further into the

235 hydraulically smooth regime. We suggest that this style of evolution would be most characteristic of  
236 channels near the terminus of submarine transport systems, on terminal lobes on the basin flow where  
237 sediment is delivered by depletive flows that are unable to re-entrain sediment.

## 238 **CONCLUSIONS**

239 It is extremely challenging to connect current-bed interactions to the temporal evolution of  
240 submarine channels in natural settings (Khripounoff et al., 2003; Xu et al., 2004, 2013; Xu, 2010; Hughes  
241 Clarke, 2016; Symons et al., 2017; Azpiroz-Zabala et al., 2017b, 2017a). We used 3 experiments in which  
242 we relate near bed turbulence, as a function of evolving bed roughness, to patterns of erosion and  
243 deposition. In all three experiments presented here, channel sinuosity influenced patterns of erosion and  
244 deposition. Although the currents used in all three case displayed shear stresses high enough to suspended  
245 sediment, the temporal evolution in the turbulence near-bed boundary layer was also very important in  
246 deciding whether the channel evolved through erosion or deposition. In the experiments where the  
247 boundary layer was transitionally rough the channel evolved through erosion, developing a roughened  
248 bed. In both cases, the near-bed boundary layer roughened from smooth or transitionally rough to rough,  
249 enhancing near-bed turbulence. When the channel substrate was cohesive, the channel bed evolved  
250 through detachment-limited erosion and most of the sediment left the system in suspension. The channel  
251 bed was patterned by erosional bedforms, grooves, inner-bank terraces and a semi-continuous inner  
252 channels. When the sediment was non-cohesive, the erosion was limited by the ability of the currents to  
253 transport sediment and the channel bed evolved into trains of ripples. In contrast, the channel with a  
254 hydraulically smooth boundary layer evolved through consistent deposition and the boundary layer  
255 appears to have remained hydraulically smooth. To our knowledge, this work presents the first instance in  
256 which detachment-limited erosional channels with realistic sediment transport patterns and sediment-  
257 turbulence interactions have been designed successfully in laboratory settings. Our results suggest that  
258 erosion in submarine channels is a self-reinforcing mechanism whereby developing bed roughness  
259 increases turbulence at the boundary layer, enhancing erosion and inhibiting deposition; deposition in

260 submarine channels occurs if the boundary layer is smooth, promoting channel aggradation and loss of  
261 channel relief.

## 262 **Acknowledgements**

263 We thank the Jackson School of Geosciences, the CSM-UT RioMAR Industry Consortium, and  
264 Shell International Exploration and Production Inc. for facilities and financial support of this work.

## 265 **References cited**

- 266 Alexander, J., McLelland, S.J., Gray, T.E., Vincent, C.E., Leeder, M.R., and Ellett, S., 2007, Laboratory  
267 sustained turbidity currents form elongate ridges at channel mouths: Channel mouth deposition from  
268 sustained turbidity currents: *Sedimentology*, v. 55, p. 845–868, doi:10.1111/j.1365-  
269 3091.2007.00923.x.
- 270 Amos, K.J., Peakall, J., Bradbury, P.W., Roberts, M., Keevil, G., and Gupta, S., 2010, The influence of  
271 bend amplitude and planform morphology on flow and sedimentation in submarine channels: *Marine*  
272 *and Petroleum Geology*, v. 27, p. 1431–1447, doi:10.1016/j.marpetgeo.2010.05.004.
- 273 Arfaie, A., Burns, A.D., Dorrell, R.M., Ingham, D.B., Eggenhuisen, J.T., and McCaffrey, W.D., 2018,  
274 Optimisation of flow resistance and turbulent mixing over bed forms: *Environmental Modelling &*  
275 *Software*, v. 107, p. 141–147, doi:10.1016/j.envsoft.2018.06.002.
- 276 Azpiroz-Zabala, M., Cartigny, M.J.B., Sumner, E.J., Clare, M.A., Talling, P.J., Parsons, D.R., and  
277 Cooper, C., 2017a, A General Model for the Helical Structure of Geophysical Flows in Channel  
278 Bends: General model for helical flows in bends: *Geophysical research letters*, v. 44, p. 11,932–  
279 11,941, doi:10.1002/2017GL075721.
- 280 Azpiroz-Zabala, M., Cartigny, M.J.B., Talling, P.J., Parsons, D.R., Sumner, E.J., Clare, M.A., Simmons,  
281 S.M., Cooper, C., and Pope, E.L., 2017b, Newly recognized turbidity current structure can explain  
282 prolonged flushing of submarine canyons: *Science advances*, v. 3, p. e1700200,  
283 doi:10.1126/sciadv.1700200.
- 284 Baas, J.H., Van Kesteren, W., and Postma, G., 2004, Deposits of depletive high-density turbidity currents:  
285 a flume analogue of bed geometry, structure and texture: *Sedimentology*, v. 51, p. 1053–1088,  
286 doi:10.1111/j.1365-3091.2004.00660.x.
- 287 Babonneau, N., Savoye, B., Cremer, M., and Bez, M., 2010, Sedimentary Architecture in Meanders of a  
288 Submarine Channel: Detailed Study of the Present Congo Turbidite Channel (Zaiango Project):  
289 *Journal of Sedimentary Research*, v. 80, p. 852–866, doi:10.2110/jsr.2010.078.
- 290 Bagnold, R.A., 1966, *An Approach to the Sediment Transport Problem from General Physics*: U.S.  
291 Government Printing Office
- 292 Cantelli, A., Pirmez, C., Johnson, S., and Parker, G., 2011, Morphodynamic and Stratigraphic Evolution  
293 of Self-Channelized Subaqueous Fans Emplaced by Turbidity Currents: *Journal of Sedimentary*  
294 *Research*, v. 81, p. 233–247, doi:10.2110/jsr.2011.20.

- 295 Cartigny, M.J.B., Eggenhuisen, J.T., Hansen, E.W.M., and Postma, G., 2013, Concentration-dependent  
296 flow stratification in experimental high-density turbidity currents and their relevance to turbidite  
297 facies models: *Journal of Sedimentary Research*, v. 83, p. 1047–1065
- 298 Conway, K.W., Barrie, J.V., Picard, K., and Bornhold, B.D., 2012, Submarine channel evolution: active  
299 channels in fjords, British Columbia, Canada: *Geo-Marine Letters*, v. 32, p. 301–312,  
300 doi:10.1007/s00367-012-0280-4.
- 301 Edmonds, D.A., Shaw, J.B., and Mohrig, D., 2011, Topset-dominated deltas: A new model for river delta  
302 stratigraphy: *Geology*.
- 303 Eggenhuisen, J.T., and McCaffrey, W.D., 2012, The vertical turbulence structure of experimental  
304 turbidity currents encountering basal obstructions: implications for vertical suspended sediment  
305 distribution in non-equilibrium currents: *Sedimentology*, v. 59, p. 1101–1120, doi:10.1111/j.1365-  
306 3091.2011.01297.x.
- 307 Eggenhuisen, J.T., McCaffrey, W.D., Haughton, P.D.W., and Butler, R.W.H., 2010, Small-Scale Spatial  
308 Variability in Turbidity-Current Flow Controlled by Roughness Resulting from Substrate Erosion:  
309 Field Evidence for a Feedback Mechanism: *Journal of Sedimentary Research*, v. 80, p. 129–136,  
310 doi:10.2110/jsr.2010.014.
- 311 Fernandes, A.M., Mohrig, D., and Buttles, J., 2018, A New Mechanism for Terrace Formation in  
312 Submarine Canyons: *EarthArXiv*. September, v. 1, doi: 10.31223/osf.io/a6p7y
- 313 Garcia, M.H., 2008, *Sedimentation Engineering: Theories, Measurements, Modeling and Practice:*  
314 *Processes, Management, Modeling, and Practice (Asce Manual and Reports on Engineering Practice*  
315 *No: American Society of Civil Engineers.*
- 316 Garcia, M., and Parker, G., 1989, Experiments on hydraulic jumps in turbidity currents near a canyon-fan  
317 transition: *Science*, v. 245, p. 393–396, doi:10.1126/science.245.4916.393.
- 318 Howard, A.D., 1994, A detachment-limited model of drainage basin evolution: *Water resources research*,  
319 v. 30, p. 2261–2285, doi:10.1029/94WR00757.
- 320 Howard, A.D., 1980, Thresholds in river regimes: *Thresholds in geomorphology*, p. 227–258.
- 321 Hughes Clarke, J.E., 2016, First wide-angle view of channelized turbidity currents links migrating cyclic  
322 steps to flow characteristics: *Nature communications*, v. 7, p. 11896, doi:10.1038/ncomms11896.
- 323 Janocko, M., Cartigny, M.B.J., Nemec, W., and Hansen, E.W.M., 2013, Turbidity current hydraulics and  
324 sediment deposition in erodible sinuous channels: Laboratory experiments and numerical  
325 simulations: *Marine and Petroleum Geology*, v. 41, p. 222–249,  
326 doi:10.1016/j.marpetgeo.2012.08.012.
- 327 Johnson, J.P., and Whipple, K.X., 2007, Feedbacks between erosion and sediment transport in  
328 experimental bedrock channels: *Earth Surface Processes and Landforms*, v. 32, p. 1048–1062,  
329 doi:10.1002/esp.1471.
- 330 Johnson, J.P.L., Whipple, K.X., Sklar, L.S., and Hanks, T.C., 2009, Transport slopes, sediment cover, and  
331 bedrock channel incision in the Henry Mountains, Utah: *Journal of geophysical research*, v. 114, p.  
332 W12446, doi:10.1029/2007JF000862.
- 333 Kane, I.A., McCaffrey, W.D., and Peakall, J., 2008, Controls on sinuosity evolution within submarine

- 334 channels: *Geology*, v. 36, p. 287–290, doi:10.1130/G24588A.1.
- 335 Khripounoff, A., Vangriesheim, A., Babonneau, N., Crassous, P., Dennielou, B., and Savoye, B., 2003,  
336 Direct observation of intense turbidity current activity in the Zaire submarine valley at 4000 m water  
337 depth: *Marine geology*, v. 194, p. 151–158, doi:10.1016/S0025-3227(02)00677-1.
- 338 Leeder, M.R., and Bridges, P.H., 1975, Flow separation in meander bends: *Nature*, v. 253, p. 338,  
339 doi:10.1038/253338a0.
- 340 de Leeuw, J., Eggenhuisen, J.T., and Cartigny, M.J.B., 2016, Morphodynamics of submarine channel  
341 inception revealed by new experimental approach: *Nature communications*, v. 7, p. 10886,  
342 doi:10.1038/ncomms10886.
- 343 Luthi, S. an, 1981, Experiments on non-channelized turbidity currents and their deposits: *Marine geology*,  
344 v. 40, p. M59–M68, doi:10.1016/0025-3227(81)90139-0.
- 345 Métivier, F., Lajeunesse, E., and Cacas, M.-C., 2005, Submarine Canyons in the Bathtub: *Journal of*  
346 *Sedimentary Research*, v. 75, p. 6–11, doi:10.2110/jsr.2005.002.
- 347 Middleton, G.V., 1966, Small-scale models of turbidity currents and the criterion for auto-suspension:  
348 *Journal of Sedimentary Research*, v. 36, p. 202–208, doi:10.1306/74D71442-2B21-11D7-  
349 8648000102C1865D.
- 350 Mitchell, N.C., 2014, Bedrock erosion by sedimentary flows in submarine canyons: *Geosphere*, v. 10, p.  
351 892–904, doi:10.1130/GES01008.1.
- 352 Mohrig, D., and Buttles, J., 2007, Deep turbidity currents in shallow channels: *Geology*, v. 35, p. 155–  
353 158, doi:10.1130/G22716A.1.
- 354 Nino, Y., Lopez, F., and Garcia, M., 2003, Threshold for particle entrainment into suspension:  
355 *Sedimentology*, v. 50, p. 247–263, doi:10.1046/j.1365-3091.2003.00551.x.
- 356 Nittrouer, J.A., Mohrig, D., and Allison, M., 2011a, Punctuated sand transport in the lowermost  
357 Mississippi River: *Journal of geophysical research*, v. 116, p. F04025, doi:10.1029/2011JF002026.
- 358 Nittrouer, J.A., Mohrig, D., Allison, M.A., and Peyret, A.-P.B., 2011b, The lowermost Mississippi River:  
359 a mixed bedrock-alluvial channel: *Sedimentology*, v. 58, p. 1914–1934, doi:10.1111/j.1365-  
360 3091.2011.01245.x.
- 361 Pirmez, C., Beaubouef, R.T., Friedmann, S.J., and Mohrig, D.C., 2000, Equilibrium profile and baselevel  
362 in submarine channels: examples from Late Pleistocene systems and implications for the architecture  
363 of deepwater reservoirs, *in* *Global deep-water reservoirs: Gulf Coast Section SEPM Foundation 20th*  
364 *Annual Bob F. Perkins Research Conference*, p. 782–805.
- 365 Rowland, J.C., Hilley, G.E., and Fildani, A., 2010, A Test of Initiation of Submarine Leveed Channels by  
366 Deposition Alone: *Journal of Sedimentary Research*, v. 80, p. 710–727, doi:10.2110/jsr.2010.067.
- 367 Shepherd, R.G., and Schumm, S.A., 1974, Experimental Study of River Incision: *GSA Bulletin*, v. 85, p.  
368 257–268, doi:10.1130/0016-7606(1974)85<257:ESORI>2.0.CO;2.
- 369 Shields, A., 1936, Anwendung der Aehnlichkeitsmechanik und der Turbulenzforschung auf die  
370 Geschiebebewegung: PhD Thesis Technical University Berlin.

- 371 Sklar, L.S., and Dietrich, W.E., 2004, A mechanistic model for river incision into bedrock by saltating  
372 bed load: *Water resources research*, v. 40, doi: 10.1029/2003WR002496.
- 373 Smith, J.D., and Hopkins, T.S., 1971, *Sediment Transport on the Continental Shelf Off of Washington*  
374 *and Oregon in Light of Recent Current Measurements: Washington Univ., Seattle. Dept. of*  
375 *Oceanography. Atomic Energy Commission, U. S. A.*
- 376 Straub, K.M., Mohrig, D., Buttles, J., McElroy, B., and Pirmez, C., 2011, Quantifying the influence of  
377 channel sinuosity on the depositional mechanics of channelized turbidity currents: A laboratory  
378 study: *Marine and Petroleum Geology*, v. 28, p. 744–760, doi:10.1016/j.marpetgeo.2010.05.014.
- 379 Straub, K.M., Mohrig, D., McElroy, B., and Buttles, J., 2008, Interactions between turbidity currents and  
380 topography in aggrading sinuous submarine channels: A laboratory study: *GSA Bulletin today: a*  
381 *publication of the Geological Society of America*, doi: 120/3-4/368/2260.
- 382 Symons, W.O., Sumner, E.J., Paull, C.K., Cartigny, M.J.B., Xu, J.P., Maier, K.L., Lorenson, T.D., and  
383 Talling, P.J., 2017, A new model for turbidity current behavior based on integration of flow  
384 monitoring and precision coring in a submarine canyon: *Geology*, v. 45, p. 367–370,  
385 doi:10.1130/G38764.1.
- 386 Vachtman, D., Mitchell, N., and Gawthorpe, R., 2013, Morphologic signatures in submarine canyons and  
387 gullies, central USA Atlantic continental margins: v. 41, p. 250–263,  
388 doi:10.1016/j.marpetgeo.2012.02.005.
- 389 van Rijn Leo C., 1984, *Sediment Transport, Part III: Bed forms and Alluvial Roughness: Journal of*  
390 *Hydraulic Engineering*, v. 110, p. 1733–1754, doi:10.1061/(ASCE)0733-9429(1984)110:12(1733).
- 391 Weill, P., Lajeunesse, E., Devauchelle, O., Métiver, F., Limare, A., Chauveau, B., and Mouazé, D., 2014,  
392 *Experimental investigation on self-channelized erosive gravity currents: Journal of Sedimentary*  
393 *Research*, v. 84, p. 487–498. Doi: 84/6/487/145405.
- 394 Whipple, K.X., 2004, *Bedrock Rivers and the Geomorphology of Active Orogens: Annual review of earth*  
395 *and planetary sciences*, v. 32, p. 151–185, doi:10.1146/annurev.earth.32.101802.120356.
- 396 Whipple, K.X., Hancock, G.S., and Anderson, R.S., 2000, River incision into bedrock: Mechanics and  
397 relative efficacy of plucking, abrasion, and cavitation: *GSA Bulletin*, v. 112, p. 490–503,  
398 doi:10.1130/0016-7606(2000)112<490:RIIBMA>2.0.CO;2.
- 399 Xu, J.P., 2010, Normalized velocity profiles of field-measured turbidity currents: *Geology*, v. 38, p. 563–  
400 566, doi:10.1130/G30582.1.
- 401 Xu, J.P., Barry, J.P., and Paull, C.K., 2013, Small-scale turbidity currents in a big submarine canyon:  
402 *Geology*, v. 41, p. 143–146, doi:10.1130/G33727.1.
- 403 Xu, J.P., Noble, M.A., and Rosenfeld, L.K., 2004, In-situ measurements of velocity structure within  
404 turbidity currents: *Geophysical research letters*, v. 31, doi:10.1029/2004GL019718.
- 405 Yu, B., Cantelli, A., Marr, J., Pirmez, C., O’Byrne, C., and Parker, G., 2006, Experiments on Self-  
406 Channelized Subaqueous Fans Emplaced by Turbidity Currents and Dilute Mudflows: *Journal of*  
407 *Sedimentary Research*, v. 76, p. 889–902, doi:10.2110/jsr.2006.069.

408

409 **Figures and captions:**

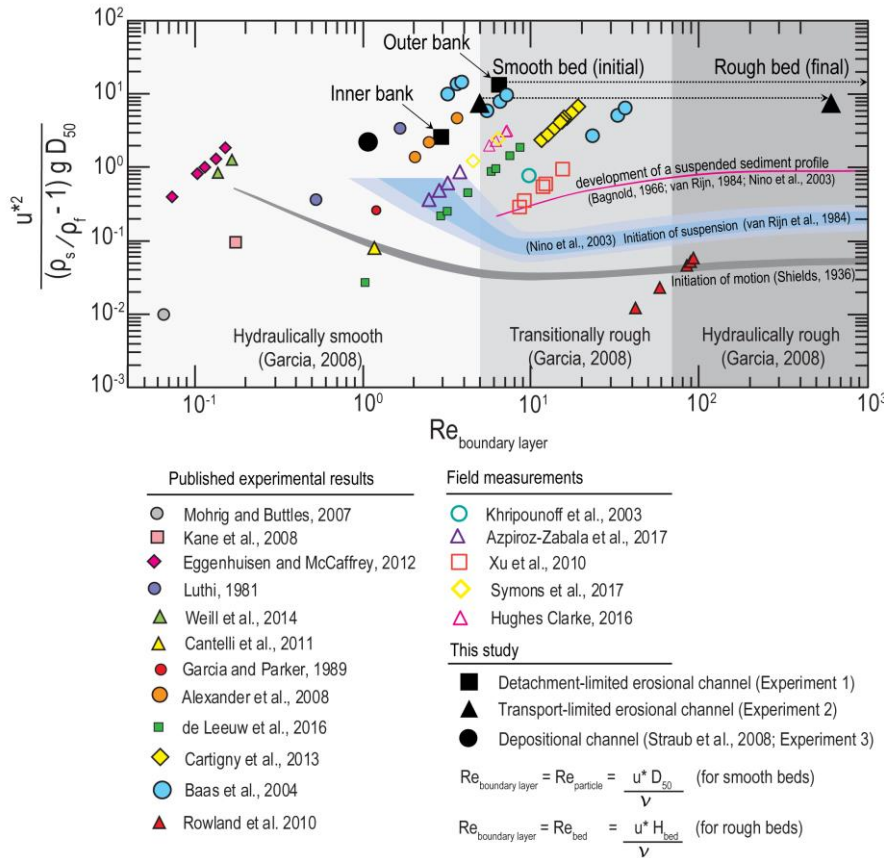


Figure 2: The modified Shield's scaling approach of de Leeuw et al., 2016, used here to compare our experiments to various experimental and field studies. Note that the initial conditions in all 3 experiments presented in this study span the threshold between hydraulically smooth and transitionally rough flow. Bed roughness

423 that evolved in Experiments 1 and 2 increased the turbulence in the boundary, causing it to become  
 424 hydraulically rough. (Luthi, 1981; Garcia and Parker, 1989; Khripounoff et al., 2003; Baas et al., 2004;  
 425 Mohrig and Buttles, 2007; Alexander et al., 2007; Straub et al., 2008; Kane et al., 2008; Xu, 2010;  
 426 Rowland et al., 2010; Cantelli et al., 2011; Eggenhuisen and McCaffrey, 2012; Cartigny et al., 2013;  
 427 Weill et al., 2014; de Leeuw et al., 2016; Hughes Clarke, 2016; Symons et al., 2017; Azpiroz-Zabala et  
 428 al., 2017b). Hydraulic thresholds based on (Shields, 1936; Bagnold, 1966; van Rijn Leo C., 1984; Nino et  
 429 al., 2003; Garcia, 2008)



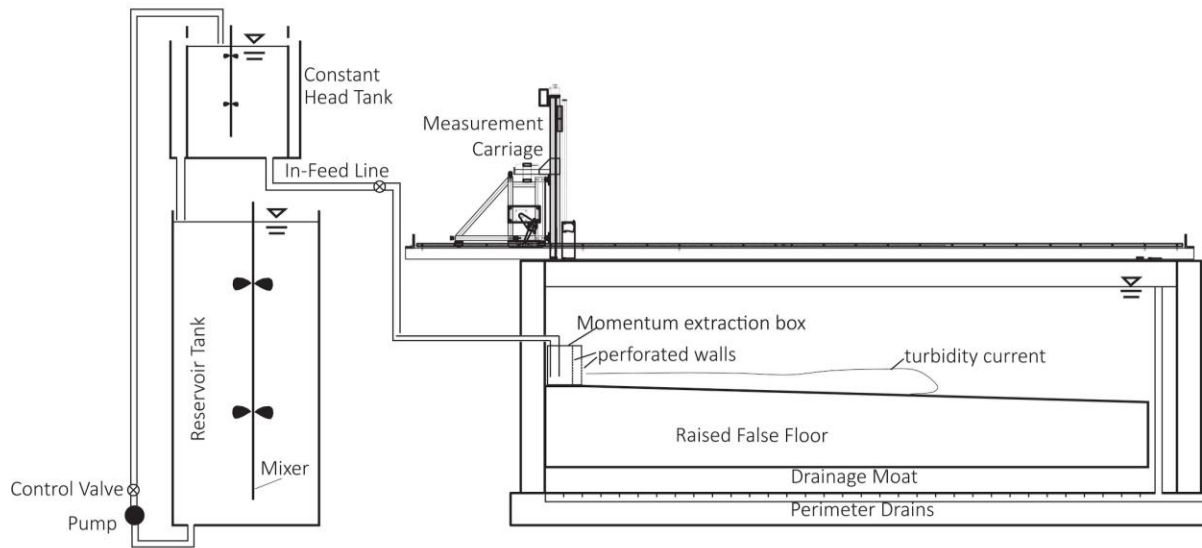


Figure 2: A generalized schematic of the experimental basin set-up used for the three experiments.

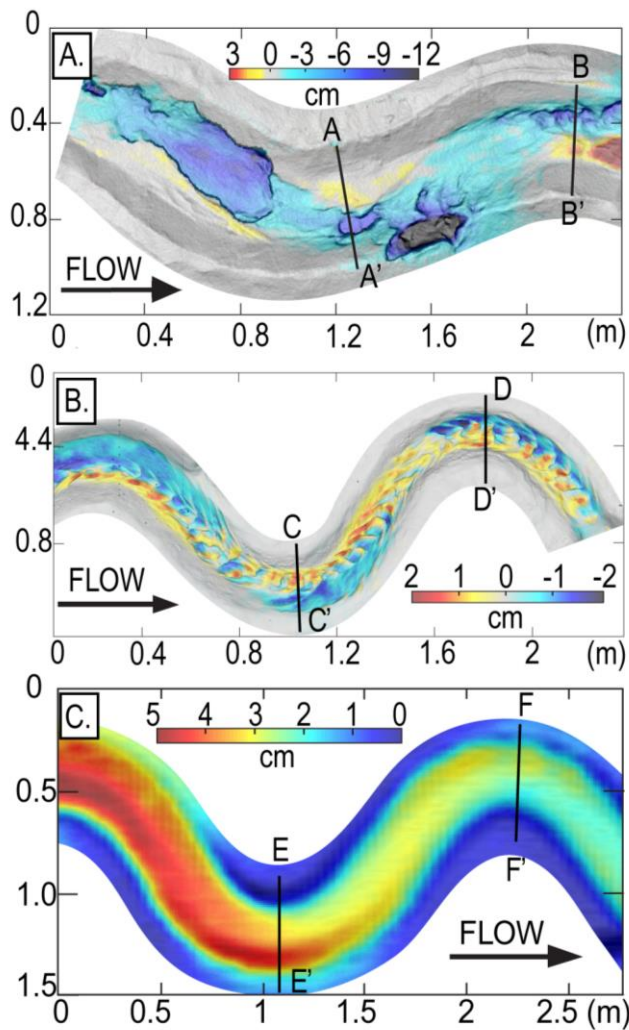


Figure 3: Difference maps defining net elevation change in all three experiments.. (A) Detachment-limited erosion in Experiment 1 resulted in a rough bed patterned with erosional bedforms along a semi-continuous erosional inner channel that followed the path of the high velocity core, and terraces formed at inner banks. (B) Transport-limited erosion in Experiment 2 resulted in a semi-continuous mobile sediment bed, reworked into ripples. (C) Consistent deposition in Experiment 3 resulted in a channel that was persistently aggradational, with the thickest deposits at the outsides of bends.

447

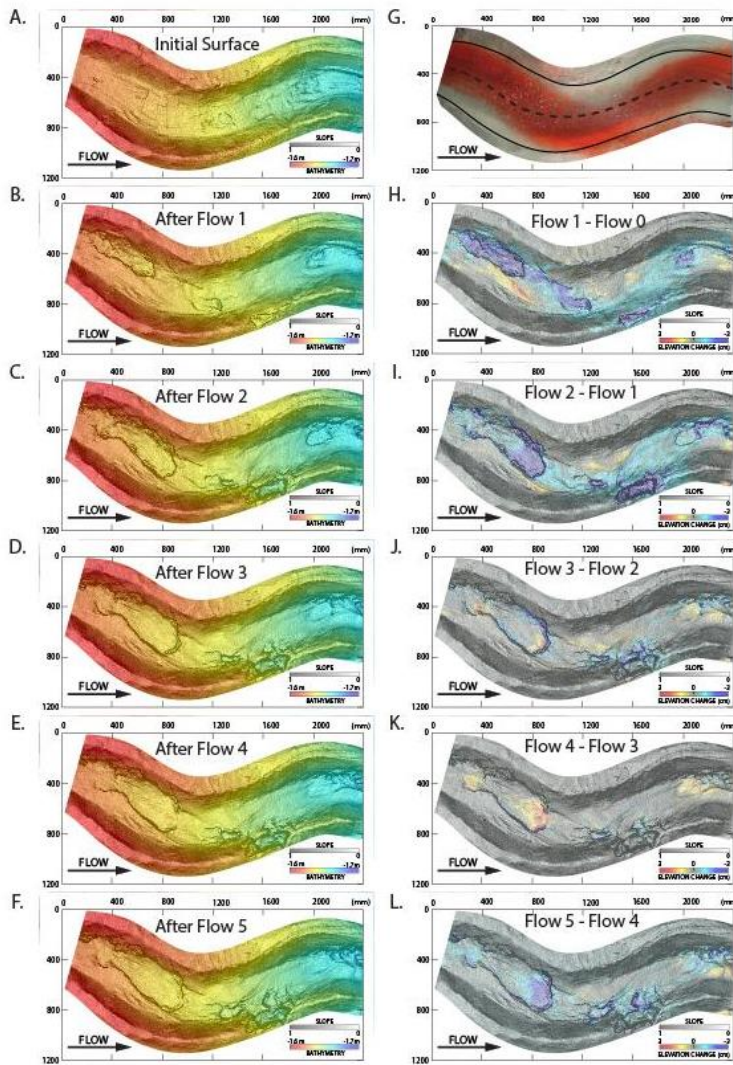


Figure 4: (A-F) Experiment 1 time-lapse laser-scanned topographic maps showing how the 5 experimental currents evolved the experimental channel. (G) Orthorectified overhead photograph showing the pathway of the high velocity core of the current-tracked by red dye with the most intensity. The very small amounts of red dye near the inner banks bear testament to very low velocities in these zones. (H-L) is a series of difference maps that define patterns of erosion and deposition within the experimental channel due to the passage of the 5 density currents. Note how erosion (cold colors) tracks the

465 pathway of the high velocity core (intense red dye in G) and no erosion weak deposition (warm colors) is  
466 associated with inner bank zones visited by separated flow (low amount of red dye in G).

467

468

469

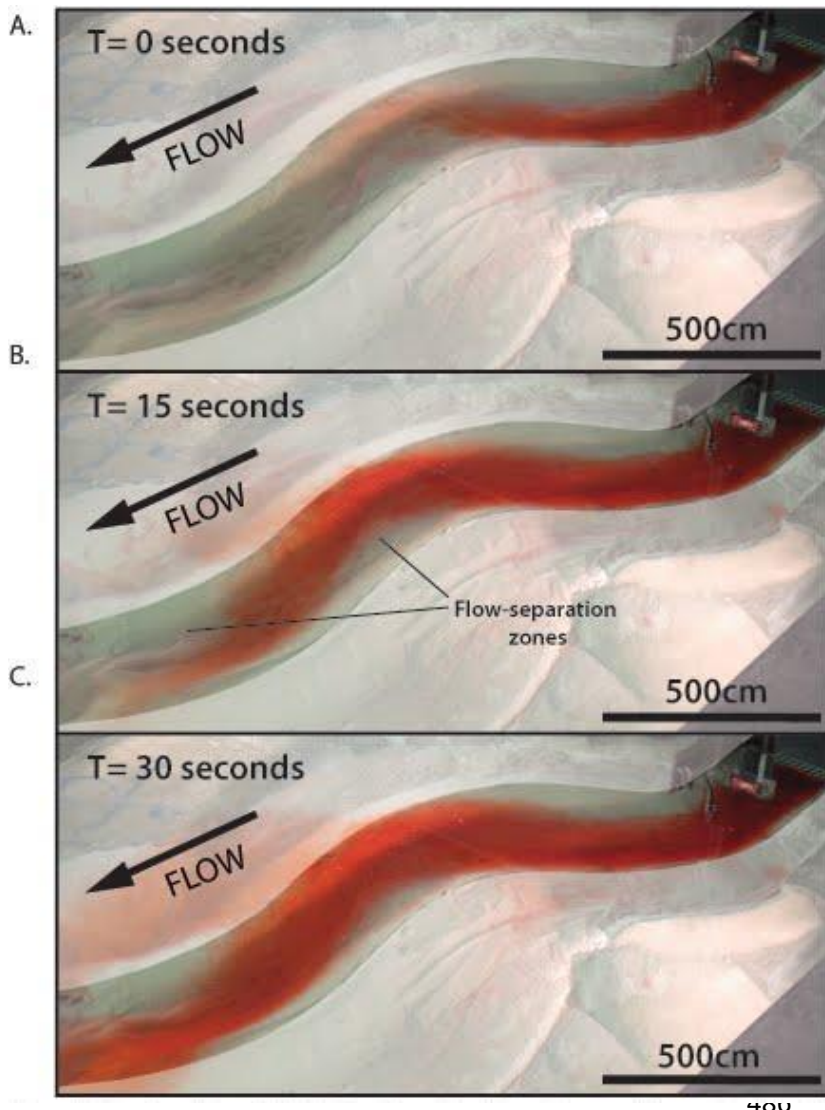
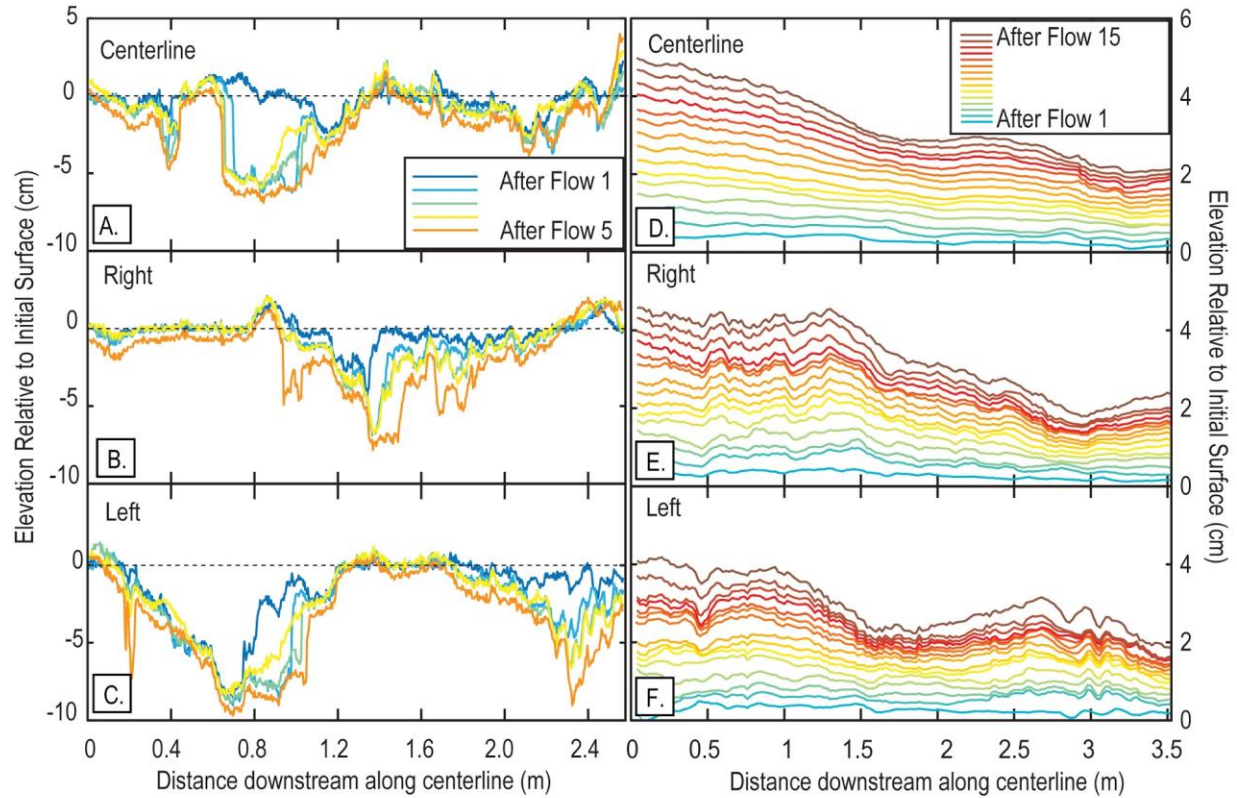


Figure 5: A-C Time lapse photographs showing a pulse of red dye in the current that defines the pathway of the high-velocity core of the current. Low velocity zones where flow separated from the inner banks received the dyed current later than the outside of bends and the dye intensity was always lower than at the outside of bends.

487

488

489



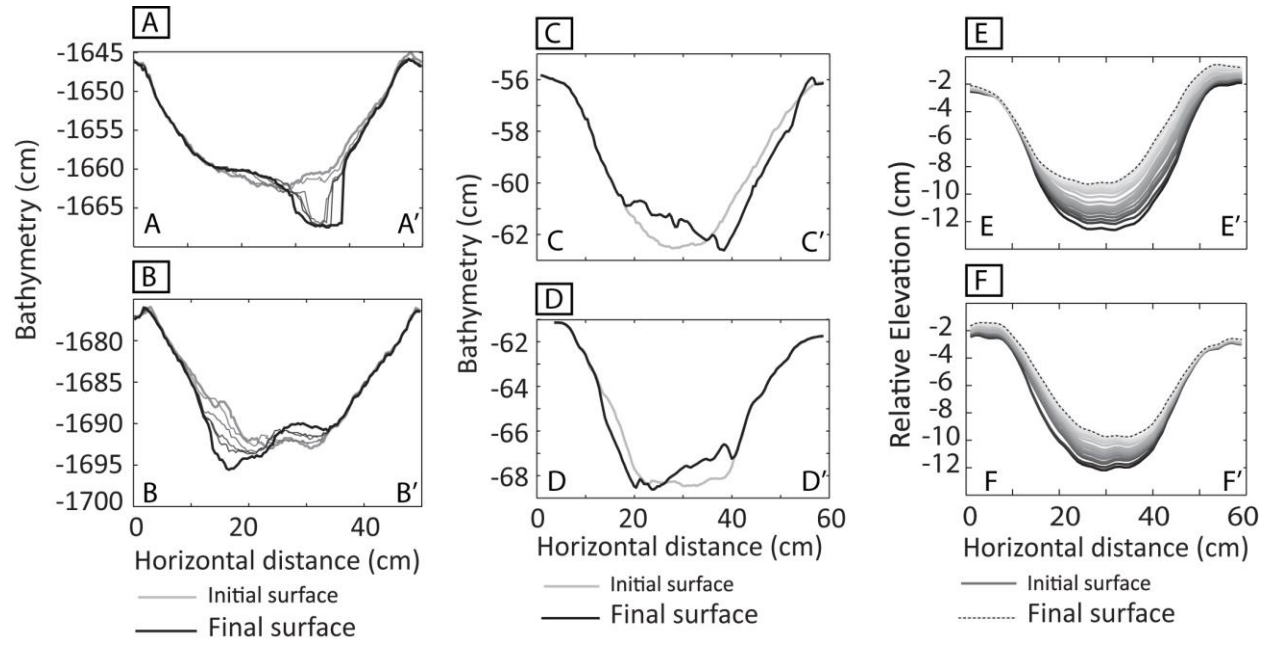
490

491 Figure 6: A-C) Change in elevation of the channel bed in Experiment 1 after the passage of 5 consecutive  
492 flows, along (A) the centerline, (B) 15 cm right of the centerline, and (C) 15 cm left of the centerline. D-  
493 F) Change in elevation of the channel bed in Experiment 3 after the passage of 15 consecutive flows,  
494 along (A) the centerline, (B) 5 cm right of the centerline, and (C) 5 cm left of the centerline.

495

496

497



498

499 Figure 7: Cross sections showing time-lapse topographic evolution at the apices of the second and third  
500 bends in Experiment 1 (A-B), Experiment 2 (C-D) and Experiment 3 (E-F).